An iron specimen of the size used by Chow *et al.*[11] was assumed. Damage reduction was 35% for irradiation by fission neutrons (average energy $\bar{E}=2$ MeV). Reductions of 32 and 22%, respectively, were obtained using a test-hole spectrum of a water-moderated reactor, $\bar{E}=0.94$ MeV, and that of a graphite-moderated reactor, $\bar{E}=0.11$ MeV.

Let us refer to the scattering approximation used in this study as the screened Coulomb hard-sphere (SHS) model and a scattering treatment using the Born-Mayer potential 2 of Gibson *et al.*[12] and the exact scattering-angle solution for this potential as the BME model. The SHS model overestimates the scattering angle in a comparison with the exact scattering angle for the screened Coulomb potential. Because of this we inferred an overly pessimistic judgement of the SHS model in a recent article[2] which should be corrected in view of subsequent results which will now be outlined. The cascade program was rewritten to accept an arbitrary potential and scattering-angle energy-transfer matrix. Calculations were then made for copper using both models and identical sets of initial conditions. The numbers of displaced atoms given by the two models agreed within 5% and the atom range given by the BME model for 1–5-keV atoms was about 20% larger than that given by the SHS model. We feel this comparison indicates that the realism of the SHS model damage results is nearly comparable to that of the BME model.

[11] J. G. Y. Chow, S. B. McRickard, and D. H. Gurinsky, *Radiation Damage in Solids* (International Atomic Energy Agency, Vienna, 1962), Vol. I, p. 277.
[12] J. B. Gibson, A. N. Goland, M. Milgram, and G. H. Vineyard, Phys. Rev. **120**, 1229 (1960).

PHYSICAL REVIEW VOLUME 134, NUMBER 2A 20 APRIL 1964

Measurement of Equilibrium Vacancy Concentrations in Dilute Aluminum-Silver Alloys*

D. R. BEAMAN, R. W. BALLUFFI, AND R. O. SIMMONS
University of Illinois, Urbana, Illinois
(Received 11 November 1963)

Precision measurements were made of the differential length expansions ($\Delta L'/L'-\Delta L^0/L^0$) and differential x-ray lattice parameter expansions ($\Delta a'/a'-\Delta a^0/a^0$) between specimens of pure aluminum and two dilute aluminum base alloys containing 0.52 and 0.94 at.% silver during slow reversible heating and cooling between the solidus and the solubility limit temperature. Absolute differences between the equilibrium vacancy concentrations in each alloy and the pure metal were then obtained from the relation

$$\Delta C_v=C_v'-C_v^0=3(\Delta L'/L'-\Delta L^0/L^0)-3(\Delta a'/a'-\Delta a^0/a^0).$$

Here, C_v is the equilibrium vacancy concentration and $\Delta L/L$ and $\Delta a/a$ are length and lattice parameter expansions. The prime and zero superscripts refer to the alloy and pure aluminum, respectively. Since C_v^0 is known from previous measurements, these differential data serve to determine C_v'. The differential length and lattice parameter measurements were carried out using the same general technique previously employed in the determination of equilibrium vacancy concentrations in a series of pure face-centered cubic metals, and yielded a relatively high precision in the determination of the extremely small differences involved. The addition of silver caused only small increases in the vacancy concentration. Values of ΔC_v equal to $(13\pm5)\times10^{-5}$ and $(12\pm5)\times10^{-5}$ were found for the 0.52 and 0.94 at.% silver alloys, respectively, at their solidus temperatures. These increments correspond to $\leqslant 23\%$ of the concentration in pure aluminum. The results for both alloys could be fitted, within the estimated uncertainty of the data, to a simple first-order vacancy-solute atom binding model, where

$$\Delta C_v=12C_sC_v^0[\exp(-S_{vs}^b/k)\exp(E_{vs}^b/kT)-1].$$

Here, C_s is the solute concentration, and the best value of the binding energy, E_{vs}^b, was found to be 0.08 eV for an assumed binding entropy $S_{vs}^b=0$. This value was of the order generally expected from previous experiments. The significance of the apparent agreement between the data and the model were discussed.

I. INTRODUCTION

ABSOLUTE measurements of the concentration of vacant atomic sites in thermal equilibrium in a number of pure face-centered cubic metals at elevated temperatures have been carried out by Simmons and Balluffi[1–4] and d'Heurle *et al.*[5] The basic method used in these measurements has been to observe the difference between the macroscopic expansion, $\Delta L/L(T_r)$,

* Supported in part by the U. S. Atomic Energy Commission Contract AT(11-1)-1198K.

[1] R. O. Simmons and R. W. Balluffi, Phys. Rev. **117**, 52 (1960).
[2] R. O. Simmons and R. W. Balluffi, Phys. Rev. **119**, 600 (1960).
[3] R. O. Simmons and R. W. Balluffi, Phys. Rev. **125**, 862 (1962).
[4] R. O. Simmons and R. W. Balluffi, Phys. Rev. **129**, 1533 (1963).
[5] F. H. d'Heurle, R. Feder, and A. S. Nowick, J. Phys. Soc. Japan **18**, 184 (1963).

and the x-ray lattice parameter expansion, $\Delta a/a(T_r)$, during slow quasiequilibrium heating to near the melting point and then to determine the total concentration of equilibrium vacant atomic sites C_v from the relation[1,6,7]

$$C_v(T)-C_v(T_r)=3[\Delta L/L(T_r)-\Delta a/a(T_r)]. \quad (1)$$

The (T_r) refers to values at a low reference temperature T_r where the equilibrium concentration is negligible. This method has the advantages that absolute equilibrium concentrations are obtained and that detailed information about the physical properties of the vacant sites is not required.[6,7]

In the present work this technique was extended to the study of equilibrium vacancy concentrations in dilute aluminum-silver alloys. It should be emphasized that Eq. (1) holds as well for the total vacancy concentration in a dilute alloy. Even though vacancies are in different environments, i.e., some are adjacent to solute atoms, each vacancy still contributes just one atomic volume to the *difference* between the macroscopic volume expansion and the lattice parameter volume expansion.[6,7] Vacancy concentration data for dilute alloys are particularly interesting, since there is a possibility that they can be understood using a simple (but approximate) nearest-neighbor model in which there is a binding energy between vacancies and solute atoms which are nearest neighbors; i.e., the formation energy of a vacancy is altered in the immediate vicinity of a solute atom. Assuming the presence of only isolated monovacancies, solute atoms, and vacancy-solute pairs, it has been shown[8,9] that

$$C_v'=C_v^0[1-12C_s+12C_s\exp(-S_{vs}^b/k) \times\exp(E_{vs}^b/kT)], \quad (2)$$

where C_v' is the total equilibrium concentration of vacant sites (monovacancies plus single vacancies bound to the solute atoms) in the alloy, C_v^0 is the equilibrium monovacancy concentration in the pure host lattice, C_s is the total solute concentration, E_{vs}^b is the vacancy-solute binding energy, and S_{vs}^b is the vibrational binding entropy. The treatment leading to Eq. (2) neglects vacancy clustering, solute clustering, and also higher order vacancy-solute clustering. It will be shown later that these approximations may be acceptable for obtaining a value of E_{vs}^b for the dilute alloys used in the present work.

The vacancy concentration is, of course, enhanced by a positive binding energy. Many previous attempts have been made to determine the effects of vacancy-solute binding on either: (1) changing the equilibrium vacancy concentration; (2) changing the apparent vacancy formation energy; or, (3) changing the rate of annealing out of nonequilibrium vacancies. In many of these experiments the apparent formation energy was reduced by dilute alloying, and also the rate of annealing out of nonequilibrium vacancies was decreased, indicating the presence of appreciable positive binding energies. A summary of some of these results, along with estimated binding energies (usually neglecting the entropy term), is given in Table I.[10–25] The derived binding energies are seen to be in the range $0<E_{vs}^b<0.85$ eV. The results for solutes in silver are in reasonable agreement with an approximate theoretical estimate[26] that $0.03<E_{vs}^b<0.24$ eV. Most of the results in Table I were obtained under often complex nonequilibrium conditions, and in some cases, assumptions were made concerning the physical properties (e.g., electrical resistivity) of the defects involved. The only previous attempt to measure C_v' under equilibrium conditions using length and lattice parameter measurements was made by d'Heurle, Feder, and Nowick[5] on several dilute lead alloys containing either indium, thallium, tin, or bismuth. They obtained the puzzling result that any vacancy concentrations in the alloys were below the level of detection even though a quite reasonable concentration was obtained for pure lead by the same technique. These results are incompatible with Eq. (2), and are not understood at present.

The results of the present work show small, but measurable, increases in the vacancy concentrations as a result of alloying, and therefore indicate a positive binding energy between vacancies and silver atoms in the aluminum matrix.

II. EXPERIMENTAL METHOD

In order to achieve the maximum possible accuracy in the present work, the difference $C_v'-C_v^0$ was measured in two alloys of increasing composition by employing a difference method. The differences between the macroscopic expansions of the alloy and the pure material were measured directly as a function of tem-

[6] R. W. Balluffi and R. O. Simmons, J. Appl. Phys. **31**, 2284 (1960).
[7] K. Fischer and H. Hahn, Z. Physik **172**, 172 (1963).
[8] A. B. Lidiard, Phil. Mag. **5**, 1171 (1960).
[9] W. M. Lomer, in *Vacancies and Other Point Defects in Metals and Alloys* (The Institute of Metals, London, 1958), p. 79.
[10] J. D. Embury and R. B. Nicholson, Acta Met. **11**, 347 (1963).
[11] C. Panseri and T. Federighi, Acta Met. **11**, 575 (1963).
[12] J. Takamura, I. G. Greenfield, and K. Okasaki, J. Phys. Soc. Japan, Suppl. III, **18**, 78 (1963).
[13] A. Eikum and G. Thomas, J. Phys. Soc. Japan Suppl. III **18**, 98 (1963).
[14] H. Kimura, A. Kimura, and R. R. Hasiguti, Acta Met. **10**, 607 (1962).
[15] K. M. Entwistle, J. H. Fell, and Kang Il Koo, J. Inst. Metals **91**, 84 (1962).
[16] H. Kimura and R. R. Hasiguti, Acta Met. **9**, 1076 (1961).
[17] K. H. Westmacott, R. S. Barnes, D. Hull, and R. E. Smallman, Phil. Mag. **6**, 929 (1961).
[18] C. Panseri and T. Federighi, Acta Met. **8**, 217 (1960).
[19] G. Thomas, Phil. Mag. **4**, 1213 (1959).
[20] Y. Quere, J. Phys. Soc. Japan Suppl. III **18**, 91 (1963).
[21] S. D. Gertsriken and B. P. Slyusar, Ukr. Fiz. Zh. **4**, 137 (1959).
[22] R. Kloske and J. W. Kauffman, Phys. Rev. **126**, 123 (1962).
[23] F. Cattaneo and E. Germagnoli, Phys. Rev. **124**, 414 (1961).
[24] Y. Hamaguchi, J. Phys. Soc. Japan **16**, 1692 (1961).
[25] S. Pearson and F. J. Bradshaw, Phil. Mag. **2**, 1387 (1957).
[26] C. P. Flynn, Phys. Rev. **125**, 881 (1962).

TABLE I. Summary of some experimental data indicating vacancy-solute atom binding.

Solvent	Solute concentration (atom percent)	$E_{vs}{}^{b}$ (eV)	Year of publication	Ref. No.
Al	(7.7 Mg) (10.2 Mg)	0.3–0.4	1963	10
Al	(4.3 Zn+0.1 Mg)	0.54±0.08	1963	11
Al	(0.1 Mg) (0.5 Mg)	0.20±0.01	1963	12
Al	(5.0 Mg)	0.1–0.4	1963	13
Al	(0.7 to 1.7 Cu)	0.15–0.25	1962	14
Al	(1.7 Cu+0.0125 In)	0.175–0.2	1962	15
Al	(1.7 Cu+0.0 to 0.05 Mg)	0.45	1962	15
Al	(1.7 Cu)	Not detectable	1962	15
Al	(1.6 Cu+0.006 Sn)	0.4–0.6	1961	16
Al	(1.2 Zn) (0.04, 1.3, 1.8 Cu) (5.4 Ag)	All less than 0.1 with Si	1961	17
Al	(1.2, 3.5, 7.3, Mg) (0.2, 0.4, 1.2 Si)	highest and Zn lowest		
Al	(4.47 Zn)	0.06	1960	18
Al	(1.0, 2.0 Cu) (1.0, 5.0 Ag)	Increase in order, Zn (lowest at	1959	19
Al	(1.0, 3.0, 5.0, 7.0 Mg) (10.0, 30.0 Zn)	≅0.06), Mg, Ag, Cu (highest)		
Ag	(0.014 oxygen)	0.3	1963	20
Ag	(0.48 Sn)	0.15±0.04	1959	21
Ag	(0.84 In)	0.24±0.04		
Au	(1.2 Ag)	<0.1	1962	22
Au	(10^{-4} to 10^{-3} Ag)	0.3	1961	23
Au	(1.8, 3.6, 5.4, 7.2 Pd)	0.85	1961	24
Pt	(1.0 Rh)	<0.16	1957	25
Pt	(0.5 Au)	<0.23		
Zn	(0.33 Cd)	0.04±0.04	1959	21

perature as were the differences between the x-ray lattice parameter expansions. Since the equilibrium concentrations in pure aluminum, $C_v{}^0$, were already known,[1] the concentrations in the alloys, $C_v{}'$, could be calculated simply from the differences. When compared to a method measuring absolute vacancy concentrations individually in each alloy,[5] the present method has the advantage that the small differences were measured directly with comparatively good precision. Since this technique appears to be potentially valuable for future studies of this type, a complete account of it is given along with an analysis of expected errors (see Appendix B).

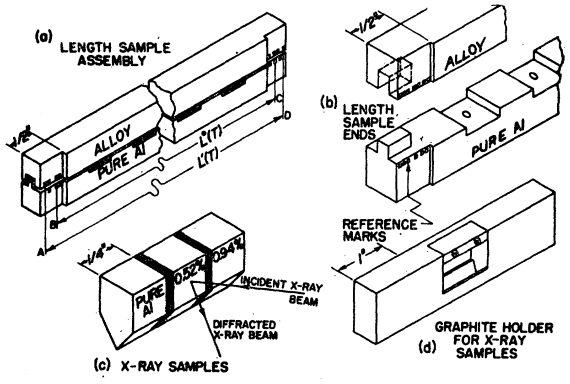

FIG. 1. Schematic drawings of the (a) length sample assembly including the pure aluminum bar, an alloy bar and the graphite spacers used for separating and positioning purposes; (b) ends of the length samples illustrating the locking mechanism; (c) three x-ray samples separated by graphite spacers; and (d) graphite x-ray specimen holder with a V-groove cavity for the three x-ray samples. All black areas are spectroscopically pure graphite spacers. Approximate dimensions are indicated.

Using Eq. (1), the difference between the vacancy concentration in the alloy and in the pure material may be written as

$$[C_v{}'(T)-C_v{}^0(T)]-[C_v{}'(T_r)-C_v{}^0(T_r)] \equiv \Delta C_v(T)-\Delta C_v(T_r)=3(\sigma-\rho), \quad (3)$$

where

$$\sigma=\Delta L'/L'(T_r)-\Delta L^0/L^0(T_r) \quad (4)$$

and

$$\rho=\Delta a'/a'(T_r)-\Delta a^0/a^0(T_r). \quad (5)$$

The quantities σ and ρ were obtained individually in separate experiments. The parameter σ was obtained by measuring the differential macroscopic expansion between an alloy bar and a pure aluminum bar over a gage length of about 50 cm during slow step heating and cooling between a temperature determined by the solubility limit and the solidus temperature of the alloy. The parameter ρ was obtained in a similar way by determining the differential x-ray lattice parameter expansion from the relative shifts of high Bragg angle reflections from alloy and pure metal single crystals, which were located in close juxtaposition, during heating. The length and x-ray specimens are shown in Fig. 1. The differential length changes were measured, as previously,[1–4] in a long precisely controlled furnace, using two parallel mounted filar micrometer telescopes. The differential lattice parameter changes were meas-

ured, as previously,[1–4] in the same furnace, using a rotating-camera back-reflection technique employing a long specimen-to-film distance.

Errors due to temperature differences were essentially eliminated in this differential technique, since the individual σ and ρ measurements were each made on sets of specimens maintained at the same temperature within the isothermal furnace enclosure. Since σ and ρ are slowly varying functions of temperature, any differences in the temperatures at which σ and ρ were measured contributed negligible error (see Appendix B, No. 8) to the determination of $\Delta C_v(T)$.

III. SPECIMEN CHEMISTRY

The alloys selected contained 0.52 and 0.94 at.% silver in aluminum. Aluminum was chosen as the base material for several reasons. Appropriate $\Delta a^0/a^0$ and $\Delta L^0/L^0$ data are available and indicate a comparatively large equilibrium vacancy concentration near the melting point. Aluminum forms a stable oxide and hence the reference marks used for following macroscopic length changes are unusually stable. Also its melting point is reasonably low and it has a low vapor pressure. In addition, previous experiments involving apparent vacancy-solute binding phenomena have been carried out in aluminum-based alloys (see Table I).

In choosing a solute, the following characteristics were sought: (a) formation of a stable alloy surface similar to that of pure aluminum; (b) an extensive range of solubility; (c) a low vapor pressure; and (d) a distribution coefficient that would permit the successful preparation of homogeneous specimens. The majority of possible solutes were eliminated by (b) and (c). Silver was finally selected as the best compromise.

Surface stability was determined in a simple oxidation experiment in which aluminum-silver alloys containing 0.0, 0.5, 1.0, and 3.0 at.% silver revealed no significant difference in weight gains when heated for 100 h at 585°C in high purity nitrogen. Surface luster was retained for all alloys during the treatment and oxide thicknesses calculated from the weight gains were less than 0.05% of the expected x-ray penetration depth.

A severe problem in obtaining specimen homogeneity existed because the x-ray volume (approximately 0.001 cm^3) constituted only a small portion of the total. In Appendix B, No. 2, the error due to a difference between the mean composition of the length measurement bar and the composition of the x-ray region is computed. In view of the magnitude of the other errors in the experiment, composition differences of less than 0.03 at.% silver were sought. Homogeneous alloy bars, approximately $1.27\times1.27\times50$ cm in length were produced[27] using a zone leveling technique. Alloy rounds were produced from 99.999% pure aluminum and silver by induction melting in spectrographically pure graphite molds under vacuum (10^{-5} mm Hg). The rounds were then swaged, placed in a graphite crucible, and zone leveled in a vertical position under vacuum (10^{-5} mm Hg). After leveling, the bars were rolled and forged to final size. Four bars, two of each composition, were produced, one bar of each composition being used for extensive destructive chemical analysis. The composition of the remaining two bars was determined by taking surface samples along the length. In order to determine the success of the zone leveling, samples were taken along the entire length. No systematic variations in composition were discovered. Nineteen samplings along one bar revealed a composition of 0.94 ± 0.02 at.% silver with a maximum deviation of 0.03%. Fifteen samplings along the second bar gave 0.52 ± 0.01 at.% silver with a maximum deviation of 0.03%. This leveling procedure, therefore, produced macroscopically homogeneous bars. Microscopic inhomogeneities were removed by long time anneals at elevated temperatures. Spectrographic analysis revealed about 90 ppm of other impurities consisting mainly of Na, Pb, Si, K, Mg, Fe, and Ca.

The pure aluminum samples were made from the same 99.995% pure material used previously.[1]

IV. LENGTH MEASUREMENTS

It was convenient to express the length expansion parameter σ [see Eq. (4)] in terms of the directly measurable quantity

$$\beta(T)=L'(T)-L^0(T), \tag{6}$$

so that

$$\sigma=\frac{L^0(T)+\beta(T)}{L^0(T_r)+\beta(T_r)}-\frac{L^0(T)}{L^0(T_r)}. \tag{7}$$

The quantity $\beta(t)$ was obtained by telescopically measuring the positions of reference marks on the ends of the specimen bars, as shown in Fig. 1(a). The long metal bars were machined[28] to fit in an interlocking assembly which, with the aid of thin spectroscopically pure graphite spacers, gave a specimen geometry in which: (1) the two bars were in close enough proximity so that reference marks on them could be seen within the 2-mm field of view of the telescope; (2) the bars were free of constraint during expansion and contraction; (3) there was no direct contact between the two bars; (4) the reference marks on the two bars were maintained in simultaneous focus by the restriction on the relative lateral movement of the two bars; and (5) any realizable specimen rotation led to only a small error in β (see Appendix B, No. 9). The surfaces on which the reference marks were made were mechanically polished prior to indenting. The marks were made with a modified Tukon microhardness tester equipped with a pyramidal diamond indenter. The resulting indenta-

[27] The two alloy bars were supplied by the Materials Research Corporation of Orangeburg, New York.

[28] The precision machining was performed by the Richardson Manufacturing Company of Springfield, Illinois.

tions were about 55 μ on an edge and retained their appearance during successive heatings and coolings.

Two runs were performed in which the lengths of the two alloy bars were individually measured relative to the pure aluminum sample. The samples were first rapidly heated in prepurified nitrogen to 525°C and held for about 50 h to allow complete solution of the silver-rich phase. Precautions were taken, during the stress relief anneals required between prior specimen machining operations, to keep the precipitated phase on as fine a scale as possible. This was accomplished by always cooling the bars rapidly at temperatures below the solubility limit. In order to remove any chemical gradients, further annealing was carried out at 625°C for 50 h. Microscopic examination of the precipitate spacing at room temperature combined with diffusion calculations indicated that this treatment yielded a homogeneous solution.

Length measurements were made during several heating and cooling runs by simultaneously measuring reference marks A and D and then B and C [Fig. 1(a)]. The temperature distribution along the length of the bar was taken just prior to and just after the completion of the telescope readings, and the mean temperature of the length measurement was determined by averaging the temperature distribution over both time and distance. In the 0.94% alloy, measurements were made from 340°C (solubility limit is 325°C)[29–31] to 636°C (solidus temperature is 643°C). In the 0.52% alloy, measurements were made from 263°C (solubility limit is 254°C) to 642°C (solidus temperature is 650°C). In order to avoid problems due to precipitation, the temperature was never decreased below the solubility temperature until all heating and cooling runs were completed. The average grain sizes in the specimens at the completion of the experiment were 17, 8, and 3 mm in the 0.00, 0.52, and 0.94 at.% silver alloys, respectively.

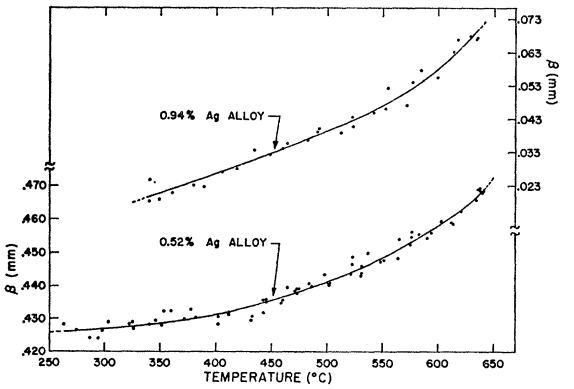

FIG. 2. Measured length differences, $\beta(T)=L'(T)-L^0(T)$, versus temperature for the 0.52 and 0.94 at.% silver alloys. Since heating and cooling measurements occurred reversibly, the data points for heating and cooling runs are not distinguished.

The values of β for the two alloys are shown in Fig. 2. No systematic lack of reversibility during heating and cooling was noted, and the heating and cooling points are therefore not differentiated. For the 0.52% alloy, the mean deviation from the smooth curve of 68 points, obtained in four heating and two cooling runs, was $\pm 1.4\,\mu$. For the 0.94% alloy, the mean deviation of 30 points, obtained in one heating and two cooling runs, was $\pm 1.7\,\mu$. (See Appendix B, No. 4, for errors caused by these deviations.)

V. X-RAY LATTICE PARAMETER MEASUREMENTS

It was convenient to express the x-ray expansion parameter ρ [see Eq. (5)] in terms of the directly measurable quantity X in the form

$$\rho=\frac{a^0(T)}{a^0(T_r)2\lambda}\left[\frac{X(T)\{k^2[a^0(T)]^2-\lambda^2\}^{1/2}}{M^0(T)}-\frac{X(T_r)\{k^2[a^0(T_r)]^2-\lambda^2\}^{1/2}}{M^0(T_r)}\right], \quad (8)$$

where X is the spacing between the diffracted lines from the alloy and the pure metal (see Appendix A for derivation and notation). In order to determine X, the diffracted beams from the pure material and the two alloy specimens [see Fig. 1(c)], at a fixed temperature, were recorded on the same film. This was accomplished using a film holder which could be driven parallel to the camera rotation axis. The three diffraction lines were then recorded one above the other in order to avoid superposition. Values of X were measured with a precision coordinate comparator. Film shrinkage corrections were found to be negligible. Ni$K\alpha_1$ radiation ($\lambda=1.65784$ Å) was diffracted from (422) planes which were parallel to the surface within two degrees.

In order to ensure that the small x-ray samples were chemically the same as the length specimens, they were cut from selected regions of the length bars after completion of the length measurements. The samples were cut with proper crystallographic orientation from regions where the deviations from the mean composition were less than 0.02 at.% silver, using an electrical discharge cutting machine. The shape of the samples [see Fig. 1(c)] was designed to allow them to be accurately positioned in the V-shaped well of the spectroscopically pure graphite holder, shown in Fig. 1(d). The samples, separated by thin graphite spacers, were free to expand but could not shift positions within the furnace causing unknown changes in the specimen to film distance. The graphite specimen holder made a tight sliding fit in the graphite furnace core (see Fig. 1 of Ref. 1).

Care was taken to obtain noncontaminated homogeneous samples of good crystal perfection. It was found that the spark cutting (with a pure aluminum electrode)

[29] M. Hanson, *Constitution of Binary Alloys* (McGraw-Hill Book Company, Inc., New York, 1958), p. 1.
[30] G. V. Raynor and D. W. Wakeman, Phil. Mag. **40**, 404 (1949).
[31] L. Rotherham and L. W. Larke, J. Inst. Metals **81**, 67 (1953).

did not yield an immediate strain-free surface.[32] Damage, as detected in Laue back reflection photographs, was found to extend about 60 μ below the cut surface, and therefore a layer of at least this thickness was etched off the x-ray faces. After placement in the furnace, the samples were given the same initial heat treatment given the length samples.

The three x-ray exposures for the three samples at a given temperature were obtained by sliding the specimen holder in the furnace core so that each sample was located at the camera rotation axis during its exposure. Each location could be exactly reproduced by observing the sample in a telescope fixed to the camera. Temperature drift during the three exposures was always maintained at less than 0.25°C and usually about 0.1°C. The temperature assigned to a film was therefore the average over the total exposure time. Measurements were carried out between 258 and 630°C.

The values of X are shown in Fig. 3 where heating and cooling data points are again not distinguished, since no evidence of systematic differences was found. In the case of the 0.52% alloy, 44 points, obtained in two heating and two cooling runs, gave a mean deviation in X of ± 0.05 mm. Forty points in the 0.94% alloy also gave a mean deviation in X of ± 0.05 mm. (See Appendix B, No. 6, for evaluation of errors caused by these deviations.)

VI. ANALYSIS OF RESULTS

Since the differential effects in the present experiment were extremely small, considerable care had to be taken in analyzing the data. Having the experimental values of β and X, the first step was to calculate σ and ρ using Eqs. (7) and (8) and reference temperatures of 250 and 325°C for the 0.52 and 0.94% alloys, respectively. The quantities β and X were only known within a certain experimental accuracy, which was assumed to be the mean deviation of the data points from the best smooth curve describing the data. Thus, the possible β values for the 0.52% silver alloy lie in a β error band, 2.8 μ wide ($\pm 1.4\,\mu$), centered on the lower curve drawn in Fig. 2. A similar band, 3.4 μ wide ($\pm 1.7\,\mu$), delineates the β values for the 0.94% silver alloy. Ranges of X values are described by X error bands, 0.1 mm wide (± 0.05 mm) centered on the curves drawn in Fig. 3.

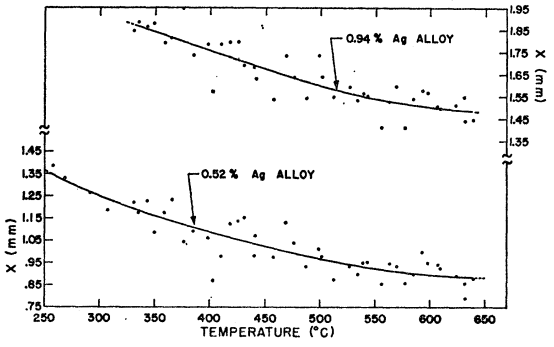

FIG. 3. Measured diffraction line separations, $X(T)$, versus temperature for the 0.52 and 0.94 at.% silver alloys. X is the distance on the film between the pure aluminum and the alloy Laue-Bragg diffraction lines (see Fig. 8). Since heating and cooling measurements occurred reversibly, the data points for heating and cooling runs are not distinguished.

[32] P. Hirsch, J. Lally, and J. Steeds, in *Electron Microscopy*, edited by S. S. Breese, Jr. (Academic Press Inc., New York, 1962), Vol. 1, p. 31.

In order to obtain maximum possible values of σ in the calculations, using Eq. (7), values of β were obtained from smooth monotonic β curves of maximum possible slope lying within the β error bands. Minimum possible values of σ were obtained from β curves of minimum possible slope. Corresponding maximum and minimum values of ρ were obtained by similar procedures using X curves of minimum and maximum slopes within the X error bands. Having these values, maximum and minimum values of the quantity $(\sigma-\rho)$ were obtained by combining the appropriate maximum and minimum values of σ and ρ. In order to ascertain the limits defined by the experimental data, maximum and minimum values of the quantity $\Delta C_v(T)-\Delta C_v(T_r)$ were then calculated using Eq. (3).

It is noted at this point that the present experiment is only capable of measuring, on an absolute basis, the quantity $[\Delta C_v(T)-\Delta C_v(T_r)]$, whereas the quantity desired is the vacancy increment at T, i.e., $\Delta C_v(T)$. This problem is not a serious one, however, since in any physically reasonable model $\Delta C_v(T_r)$ should be relatively small if T_r is chosen sufficiently low. We therefore proceed by defining a new parameter η, where

$$3\eta = 3\sigma + \Delta C_v(T_r), \tag{9}$$

so that

$$\Delta C_v(T) = 3(\eta-\rho). \tag{10}$$

The problem is therefore to pick values of the small quantity $\Delta C_v(T_r)$ so that $\Delta C_v(T)$ is always positive and approaches a zero value at the low reference temperature employed. In order to obtain best results, it was necessary to employ values of $\Delta C_v(T_r)$ ranging from 0.06 to 1.6×10^{-5}. The final maximum and minimum values of η and ρ are shown in Figs. 4 and 5. It is seen that it was not possible to satisfy the above criteria for $\Delta C_v(T)$ in the low-temperature range for all cases. In some cases the curves represent estimated best compromises between relatively large values of $\Delta C_v(T_r)$ and negative values of $\Delta C_v(T)$ in the temperature range of 300–500°C. The maximum and minimum possible vacancy increments were obtained from the smooth curves in Figs. 4 and 5 and are shown in Figs. 6 and 7. The shaded regions in Figs. 6 and 7 indicate the ranges of uncertainty in the vacancy increments which, of course, were derived from our original assumption that the uncertainty in Figs. 2 and 3 is given by $\pm$ the mean deviation of the data points from the smooth curves.

The results in Figs. 6 and 7 show that the addition of

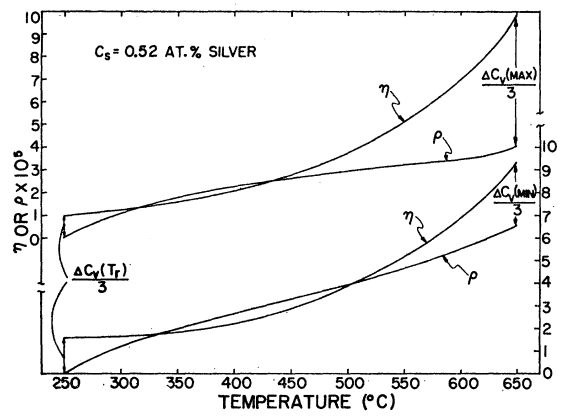

FIG. 4 η and ρ versus temperature for the 0.52-at.% silver alloy. The upper and lower sets of curves represent conditions that yield the maximum and minimum values, respectively, of the vacancy increment, $\Delta C_v(T)=3(\eta-\rho)$.

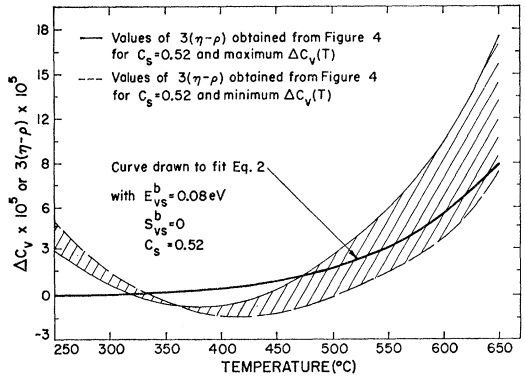

FIG. 6. $\Delta C_v(T)$ versus temperature for the 0.52-at.% silver alloy. The upper and lower curves, along with the shaded area, define the range of uncertainty derived from ± the mean deviations of the data points in Figs. 2 and 3. The indicated curve represents the best fit to Eq. (2) using $E_{vs}{}^b=0.08$ eV and $S_{vs}{}^b=0$.

silver at the concentrations used caused only small relative increases in the equilibrium vacancy concentrations. The increments are seen to increase with temperature from values which are near zero at T_r. At the highest temperature $8.3\times10^{-5}<\Delta C_v(650)<17.4\times10^{-5}$ for the 0.52% silver alloy, and $6.9\times10^{-5}<\Delta C_v(643)<17.6\times10^{-5}$ for the 0.94% silver alloy. These increments represent a 9 to 23% increase in vacancy content over that in pure aluminum. The ranges of uncertainty in Figs. 6 and 7 are in good agreement with our estimated total error, accrued from all sources, which has been calculated in Appendix B on the assumption of a model obeying Eq. (2) and possessing vacancy increments of the magnitude found experimentally. This good agreement indicates that the uncertainty ranges in Figs. 6 and 7 are realistic.

We note in Fig. 6 (0.52% alloy) that several fairly appreciable deviations occur from the expected small values at low temperatures. It is seen in Fig. 4 that this behavior stems from the low-temperature divergence of the ρ and η curves. The reason for the existence of these small differences is unknown. It is emphasized that the data point population is lowest near the lower temperature limit of the present work and that the uncertainty in the curve position is greatest there. Also, the magnitudes of these low-temperature deviations are small in comparison to the total effect at higher temperatures. It therefore seems reasonable to disregard them.

VII. MODELS

It was of interest to fit the vacancy increment data in Figs. 6 and 7 to the first-order model represented by Eq. (2). The best fit calculated from Eq. (2) on the assumption that $S_{vs}{}^b=0$ is shown in Figs. 6 and 7 and corresponds to a binding energy $E_{vs}{}^b=0.08$ eV. (Varying $E_{vs}{}^b$ from this value by more than about ±0.01 eV caused the calculated curves to fall outside of the uncertainty ranges.) These results indicate that the present data fit the simple first-order model within

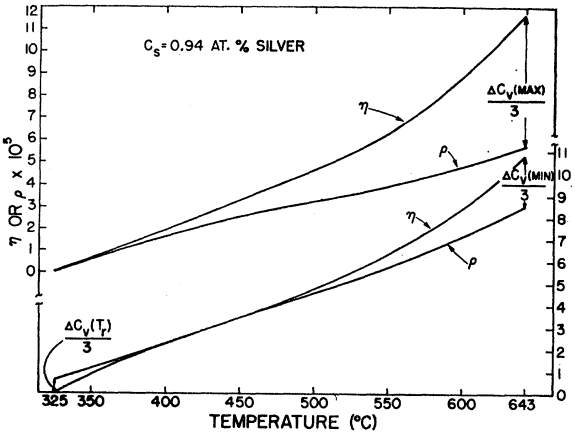

FIG. 5. η and ρ versus temperature for the 0.94 at.% silver alloy. The upper and lower sets of curves represent conditions that yield the maximum and minimum values, respectively, of the vacancy increment, $\Delta C_v(T)=3(\eta-\rho)$.

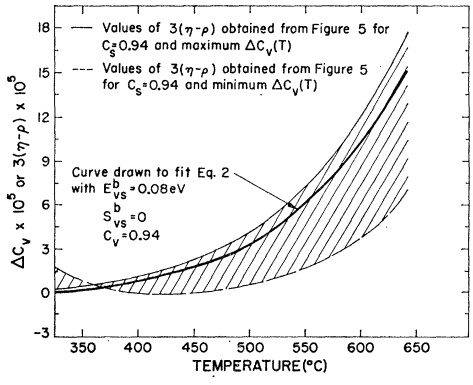

FIG. 7. $\Delta C_v(T)$ versus temperature for the 0.94 at.% silver alloy. The upper and lower curves, along with the shaded area, define the range of uncertainty derived from ± the mean deviations of the data points in Figs. 2 and 3. The indicated curve represents the best fit to Eq. (2) using $E_{vs}{}^b=0.08$ eV and $S_{vs}{}^b=0$.

the estimated accuracy of the data. The assumption that $S_{vs}{}^b=0$ is, of course, unsupported and was made on the simple expectation that this factor is fairly small. Fits with the data can still be obtained for nonzero binding entropies, and we find for $S_{vs}{}^b=0\pm k/2$; $E_{vs}{}^b\simeq 0.08\pm 0.03$ eV, and for $S_{vs}{}^b=0\pm k$; $E_{vs}{}^b\simeq 0.08\pm 0.07$ eV.

The apparent consistency of the present data with the first-order model requires some discussion. Consider first the neglect of possible vacancy-vacancy, solute-solute, and higher order vacancy-solute complexes. Doyama and Koehler[33] have recently derived a divacancy binding energy of 0.17 eV in pure aluminum from quenching and annealing experiments. The analysis of vacancy clustering carried out in Ref. 1 indicates that with this binding energy, vacancy clustering should be unimportant.

There is, unfortunately, very little information concerning the possibility of solute-solute binding. From general thermodynamic considerations, the aluminum-silver system is expected to exhibit clustering. Evidence for the clustering of silver atoms in aluminum-silver alloys above the solubility temperature has been found in a 5 at.% silver alloy[34] and a 10 at.% silver alloy.[35] For present purposes a first-order approximation of the clustering effects can be made using quasichemical theory.[36] As pointed out by Swalin,[36] quasichemical theory may be expected to yield approximate results when the heat of mixing does not contain a large strain energy term. This should be the case in the present system where the atomic radii are 1.43 and 1.44 Å for aluminum and silver, respectively. The binding energy of two silver atoms, $E_{\text{Ag-Ag}}{}^b$ may be readily obtained in terms of the standard quasichemical energy parameter,

$$\omega=E_{\text{Ag-Al}}-(1/2)(E_{\text{Ag-Ag}}+E_{\text{Al-Al}}), \qquad (11)$$

where the energies indicated are the so-called bond energies. Consideration of the changes in bonding when two isolated silver atoms are brought together to form a nearest-neighbor pair shows that $E_{\text{Ag-Ag}}{}^b=2\omega$. Using x-ray data, Hillert *et al.*[37] obtained $\omega=0.6\,kT$ for a 10-at.% silver in aluminum alloy at 540°C. For the same alloy at the same temperature they obtained $\omega=0.1\,kT$ from heat of mixing data. Speculation concerning this difference in ω values is presented in Ref. 37. Possible values of $E_{\text{Ag-Ag}}{}^b$ are therefore 0.08 and 0.014 eV. Using these binding energies, the relative concentration of unbound silver atoms, C_{Ag}/C_s may be calculated from the relations

$$C_{\text{Ag-Ag}}\cong 6C_{\text{Ag}}{}^2\exp(E_{\text{Ag-Ag}}{}^b/kT)/(1-12C_{\text{Ag}})^2, \qquad (12)$$

TABLE II. Relative concentrations of unbound silver atoms at 500° and 650°C for three values of the silver-silver solute pair binding energy, calculated from Eqs. (12) and (13).

C_s	$E_{\text{Ag-Ag}}{}^b$ (eV)	C_{Ag}/C_s at 500°C	C_{Ag}/C_s at 650°C
0.005	0.00	0.94	0.94
0.005	0.014	0.92	0.94
0.005	0.08	0.84	0.86
0.01	0.00	0.88	0.88
0.01	0.014	0.86	0.86
0.01	0.08	0.74	0.77

and

$$C_s=C_{\text{Ag}}+2C_{\text{Ag-Ag}}. \qquad (13)$$

Here, C_{Ag}, $C_{\text{Ag-Ag}}$, and C_s are the concentrations of unbound silver atoms, silver-solute pairs, and total solute, respectively. Resulting values for various conditions are given in Table II. It is seen that the relative concentration of unbound silver atoms is fairly large and that more than 74% of the total silver atoms remain single even under the most extreme conditions.

The apparent consistency of the present data with the first-order binding model, therefore, seems reasonable on the basis of clustering considerations. The nearest-neighbor approximation neglects atomic interactions extending beyond the nearest-neighbor shell which, of course, are known to exist. However, such effects are not expected to be of overriding importance, and the present results appear to be consistent with this. In view of the present results the very definite inconsistency of the data of d'Heurle *et al.*[5] for lead and dilute lead alloys with the simple binding model remains puzzling. Further experimental work appears to be in order.

We conclude by noting that even though there is apparent consistency between the present data and the simple binding model, the present data, of course, do not serve to validate the model. The uncertainty in the data is too great for this purpose, and most probably other models yielding an increasing $\Delta C_v(T)$ with temperature could be fitted to the data. It would be of considerable interest to investigate a system with a higher binding energy so that considerably larger vacancy increments could be obtained in order to provide a more critical test of binding models.

ACKNOWLEDGMENTS

The writers wish to thank D. M. File for his help with the experimental measurements and calculations. The preparation of the x-ray samples by J. C. Burr of the Coordinated Science Laboratory is greatly appreciated.

APPENDIX A: DERIVATION OF EXPRESSION FOR ρ IN TERMS OF EXPERIMENTAL QUANTITIES

In order to obtain ρ, consider the geometry of diffraction at the two temperatures T and T_r, as in Fig. 8. We

[33] M. Doyama and J. S. Koehler (to be published).
[34] C. Walker, J. Blin, and A. Guiner, Compt. Rend. **235**, 254 (1952).
[35] P. S. Rudman and B. L. Averbach, Acta Met. **2**, 576 (1954).
[36] R. A. Swalin, *Thermodynamics of Solids* (John Wiley & Sons, Inc., New York, 1962), p. 126.
[37] M. Hillert, B. Averbach, and M. Cohen, Acta Met. **4**, 31 (1956).

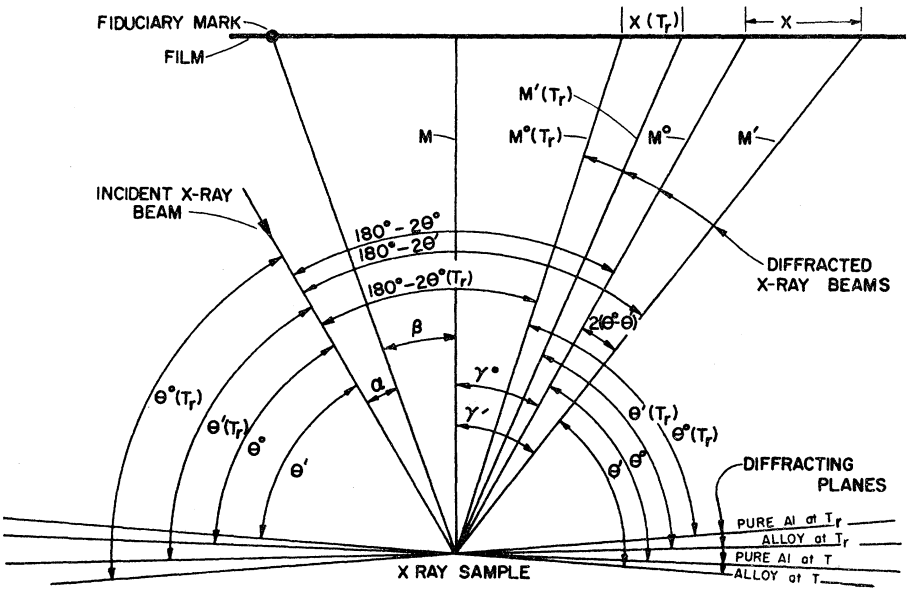

FIG. 8. X-ray diffraction geometry for the pure aluminum and one alloy sample at two different temperatures, i.e., the reference temperature T_r and a higher temperature T. All values refer to a temperature T unless otherwise indicated. α and β are constants. M is the specimen to film distance when the diffracted beam is normal to the film (505.25 mm in the experiment).

find, since γ^0 is always less than 6 degrees,

$$X(T)=2M^0(T)(\theta^0-\theta')=2M^0(T)\Delta\theta, \quad \text{(A1)}$$

where $X(T)$ is the separation on the film of the diffraction lines from the alloy and the pure material, $M(T)$ is the specimen to film distance, and $\Delta\theta$ is the difference in Bragg angles. From Bragg's law, with the wavelength constant, we obtain

$$\Delta\theta=-(\Delta d/d)\tan\theta=-(\Delta a/a)\tan\theta. \quad \text{(A2)}$$

Since the difference a^0-a' is small compared to a^0, we can write

$$\Delta\theta=\theta^0-\theta'=-\frac{(a^0-a')}{a^0}\tan\theta. \quad \text{(A3)}$$

Letting

$$\alpha(T)=a'(T)-a^0(T), \quad \text{(A4)}$$

we obtain

$$\alpha=\Delta\theta a^0/\tan\theta. \quad \text{(A5)}$$

From Bragg's law for an (hkl) plane reflection

$$\tan\theta=\lambda[k^2(a^0)^2-\lambda^2]^{-1/2}, \quad \text{(A6)}$$

where

$$k=2(h^2+k^2+l^2)^{-1/2}.$$

Combining Eqs. (A1), (A5), and (A6),

$$\alpha=[k^2(a^0)^2-\lambda^2]^{1/2}(a^0X/2M\lambda). \quad \text{(A7)}$$

Rewriting Eq. (5) in the form

$$\rho=\frac{a'(T)}{a'(T_r)}-\frac{a^0(T)}{a^0(T_r)},$$

and using Eq. (A4),

$$\rho=\frac{a^0(T)+\alpha(T)}{a^0(T_r)+\alpha(T_r)}-\frac{a^0(T)}{a^0(T_r)}. \quad \text{(A8)}$$

Expanding the first term on the right side of Eq. (A8) and neglecting all terms beyond the third, we obtain

$$\rho=[a^0(T_r)]^{-2}[\alpha(T)a^0(T_r)-\alpha(T_r)a^0(T)]. \quad \text{(A9)}$$

Combining Eqs. (A7) and (A9) yields finally Eq. (8) of the text which expresses ρ as a function of the experimental quantity X, the lattice parameter of the pure material, and parameters of the diffraction experiment.

APPENDIX B: ERROR CALCULATIONS

In the calculation of possible errors $\Delta C_v(T_r)$ is assumed negligibly small, and Eq. (3) is written as $\Delta C_v(T)=3(\sigma-\rho)$. Unless otherwise indicated, errors were computed at 650° and 643°C for the 0.52 and 0.94% silver alloys, respectively.

No. 1. Error introduced through use of the approximate solution for ρ. This error is evaluated by constructing a realistic, but tractable, model from which ρ(exact) can be determined and then working backwards to values of X from which ρ(approx) can be calculated using Eq. (8). The following equations constitute the model used:

$$\Delta a^0/a^0(T_r)=B\Delta T-C_v^0/6, \quad \text{(B1)}$$

$$\Delta a'/a'(T_r)=\varphi B\Delta T-C_v'/6, \quad \text{(B2)}$$

$$\Delta L^0/L^0(T_r)=B\Delta T+C_v^0/6, \quad \text{(B3)}$$

$$\Delta L'/L'(T_r)=\varphi B\Delta T+C_v'/6, \quad \text{(B4)}$$

$$\varphi=\alpha'(T)/\alpha^0(T), \quad \text{(B5)}$$

where $\alpha(T)$ is the thermal expansion coefficient at temperature T, and B is the pure thermal expansion contribution to $\Delta a^0/a^0$ and $\Delta L^0/L^0$ between some reference temperature T_r and the solidus temperature. From Fig. 3 in Ref. 1, B was determined to be $33.0\times10^{-6}°C^{-1}$ for the temperature range 325–650°C.

By combining Eqs. (B1) and (B2),

$$\rho(\text{exact})=\Delta a'/a'(T_r)-\Delta a^0/a^0(T_r)$$
$$=B\Delta T(\varphi-1)-(\Delta C_v)/6. \quad \text{(B6)}$$

ρ(approx) can be evaluated using Bragg's law and the geometry of diffraction shown in Fig. 8. Briefly, the procedure is as follows.

Knowing α^0(20–325), α'(20–325) is determined for an arbitrary value of φ. Since $a^0(20)$ and $a'(20)$ are equivalent for low silver concentrations,[38–40] $a'(T_r)$ is known if T_r is chosen sufficiently low. $a'(T)$ is determined by selecting arbitrary values of C_v' for use in Eq. (B2), and writing

$$a'(650)=[a'(325)][1+\Delta a'/a'(325)]. \quad \text{(B7)}$$

Knowing $a'(T)$, $\theta'(T)$ is determined from Bragg's law. From Fig. 2, $\gamma'(T)=180-2\theta'(T)-(\alpha+\beta)$, and $\gamma^0(T)=180-2\theta^0(T)-(\alpha+\beta)$. Since α and β are constants, $\gamma'(T)$ and $\gamma^0(T)$ are determined. From Fig. 2 it is evident that

$$X(650)=M[\tan\gamma'(650)-\tan\gamma^0(650)],$$
$$X(325)=M[\tan\gamma'(325)-\tan\gamma^0(325)]. \quad \text{(B8)}$$

These values of X are then substituted into Eq. (8) to obtain ρ(approx). The best estimate of the error in ρ, using the experimental data, is 0.6 ppm yielding a corresponding 1.2–2.0% error in ΔC_v(650).

No. 2. Error due to difference between the mean composition of the bar and the composition of the x-ray volume. We compare ΔC_v as determined in the following two cases: (1) The composition of the x-ray sample and the length sample are equal and given by C_s'; (2) the composition of the x-ray sample is given by $C_s''=C_s'\pm\delta C_s$, while the mean composition of the bar remains at C_s'. Let ρ' and ρ'' be the values of ρ for x-ray samples of composition C_s' and C_s'', respectively. The fractional error in ΔC_v is written

$$\frac{\delta\Delta C_v}{\Delta C_v}=\frac{3(\sigma'-\rho'')-3(\sigma'-\rho')}{3(\sigma'-\rho')}=\frac{\rho'-\rho''}{\sigma'-\rho'}.$$

From Eq. (B2),

$$\rho'-\rho''=B\Delta T(\varphi'-\varphi'')-(C_v'-C_v'')/6.$$

We assume that solute additions have a bulk effect on the expansion coefficient, i.e., φ, for an aluminum 1% silver alloy is 1.01. Then $\varphi'-\varphi''=C_s'-C_s''$. This is a generous estimate of the solute effect and therefore will make the error values calculated somewhat higher than actually expected. From Eq. (B2),

$$C_v'-C_v''=12C_v^0(C_s''-C_s')[1-\exp(E_{vs}^b/kT)].$$

Thus, the fractional error in ΔC_v due to a composition variation δC_s is

$$\frac{\delta\Delta C_v}{\Delta C_v}=(C_s'-C_s'')\times\left\{\frac{B\Delta T-2C_v^0[\exp(E_{vs}^b/kT)-1]}{4C_s'C_v^0[\exp(E_{vs}^b/kT)-1]}\right\}. \quad \text{(B9)}$$

For $C_s'=0.01$, $E_{vs}^b=0.08$ eV, and δC_s values of 0.0001, 0.0005, and 0.001, the errors in ΔC_v(650) are 1.4, 6.6, and 13.4%, respectively. For $C_s'=0.005$, corresponding errors of 2.7, 13.5, and 26.7% are obtained.

No. 3. Error due to an uncertainty in the length of the pure aluminum bar L^0(20). Differentiation of Eq. (7) yields

$$\delta\sigma=\left\{\frac{L^0(T)+\beta(T)+L^0(T_r)+\beta(T_r)}{[L^0(T_r)+\beta(T_r)]^2}-\frac{L^0(T_r)+L^0(T)}{[L^0(T_r)]^2}\right\}|\delta L^0|. \quad \text{(B10)}$$

Since δL is ±0.01 mm, this error is negligible (less than 0.01% error in ΔC_v). In the experiment, L_{20}^0 was 495.88 mm.

No. 4. Error due to a measurement error in β. Differentiation of Eq. (7) with respect to β yields

$$\delta\sigma=\left\{\frac{L^0(T_r)+\beta(T_r)+L^0(T)+\beta(T)}{[L^0(T_r)+\beta(T_r)]^2}\right\}|\delta\beta|. \quad \text{(B11)}$$

Using the mean deviation in β for $\delta\beta$, a 5.6 ppm error in σ is obtained for the 0.52% silver alloy. This corresponds to a 19% error in ΔC_v(650) if $E_{vs}^b=0.08$ eV. For the 0.94% alloy, a 6.8 ppm error in σ corresponds to a 13% error in ΔC_v(643).

No. 5. Error due to an error in the lattice parameter of the pure material a^0. Differentiating Eq. (8) with respect to a^0, and letting

$$A(T)=\{k^2[a^0(T)]^2-\lambda^2\}^{1/2},$$

and

$$A(T_r)=\{k^2[a^0(T_r)]^2-\lambda^2\}^{1/2},$$

we obtain

$$\delta\rho=\frac{1}{2\lambda}\left\{\frac{a^0(T)}{a^0(T_r)}\left[\frac{X(T)k^2a^0(T)}{M(T)A(T)}+\frac{X(T_r)k^2a^0(T_r)}{M(T_r)A(T_r)}\right]+\left[\frac{X(T)A(T)}{M(T)}-\frac{X(T_r)A(T_r)}{M(T_r)}\right]\times\left(\frac{a^0(T)+a^0(T_r)}{[a^0(T_r)]^2}\right)\right\}|\delta a^0|. \quad \text{(B12)}$$

[38] E. C. Ellwood, J. Inst. Metals **80**, 605 (1952).
[39] J. E. Dorn, P. Pietrokowsky, and T. E. Tietz, J. Inst. Metals **2**, 933 (1950).
[40] H. Axon and W. Hume-Rothery, Proc. Roy. Soc. (London) **A193**, 1 (1948).

Letting $\delta a^0 = 2\times10^{-4}$ Å, an error of 1 ppm in ρ is obtained. This leads to 3.3 and 1.9% errors in ΔC_v in the 0.52 and 0.94% alloys, respectively, for $E_{vs}{}^b = 0.08$ eV.

No. 6. Error due to an error in X. Differentiating Eq. (8) with respect to X,

$$\delta\rho = \frac{a^0(T)}{a^0(T_r)2\lambda}\left[\frac{A(T)}{M(T)} + \frac{A(T_r)}{M(T_r)}\right]|\delta X|. \quad \text{(B13)}$$

δX is ±0.05 mm for both alloys. Errors in ρ of 14 and 13 ppm for the 0.52 and 0.94% alloys, respectively, lead to a 46% error in ΔC_v for the 0.52% alloy and 25% for the 0.94% alloy, when $E_{vs}{}^b = 0.08$ eV. This error drops off rapidly as $E_{vs}{}^b$ increases, decreasing to 32% in the 0.52% alloy when $E_{vs}{}^b = 0.10$ eV.

No. 7. Error due to an uncertainty in the specimen-to-film distance M. Differentiating Eq. (8) with respect to M,

$$\delta\rho = \frac{a^0(T)}{a^0(T_r)2\lambda}[X(T)A(T) + X(T_r)A(T_r)]\frac{|\delta M|}{M^2}. \quad \text{(B14)}$$

An error of ±0.2 mm in M yields an error in ρ of approximately 0.2 ppm which causes 0.7 and 0.4% errors in ΔC_v for the 0.52 and 0.94% alloys, respectively, when $E_{vs}{}^b = 0.08$ eV.

No. 8. Error due to the fact that x-ray and length measurements are not made simultaneously. This error is introduced because of uncertainties in the temperatures measured in the separate length and x-ray runs. It can be approximated by writing,

$$\frac{\delta\Delta C_v}{\Delta C_v} = \frac{\sigma(T) - \rho(T) - \sigma(T\pm\delta T) + \rho(T)}{\sigma(T) - \rho(T)} \quad \text{or} \quad \frac{(\partial\sigma/\partial T)\delta T}{\sigma(T) - \rho(T)}. \quad \text{(B15)}$$

Letting $\delta T = 0.5$°C, errors of 0.7 and 1.7% in ΔC_v are obtained for the 0.94 and 0.52% alloys, respectively. This is the maximum possible error, since it was computed at the maximum temperature where the slope of the σ versus T curve is greatest.

No. 9. Error due to rotation of entire length sample assembly within the graphite core. The entire length sample assembly can rotate inside the graphite core in a horizontal plane about a vertical axis because of the loose sliding fit and thereby cause an error in β. At 650°C the maximum gap between the core and the sample is 0.56 mm. A geometrical solution indicates a maximum error in β of 2.8 (10^{-4}) mm, which in turn yields a 1.1 ppm error in σ. This gives 3.7 and 2.1% errors in ΔC_v for the 0.52 and 0.94% alloys, respectively.

No. 10. Error in the binding energy $E_{vs}{}^b$ due to an error in the experimental quantity $3(\sigma-\rho)$. Differentiating Eq. (2),

$$\frac{\delta E_{vs}{}^b}{E_{vs}{}^b} = \frac{\delta\Delta C_v}{\Delta C_v}\frac{kT[\exp(E_{vs}{}^b/kT) - 1]}{E_{vs}{}^b\exp(E_{vs}{}^b/kT)}. \quad \text{(B16)}$$

Using the most probable error in $\Delta C_v(650)$ calculated from errors 1 to 9 above, 16.8 and 31.9% errors in $E_{vs}{}^b$ were obtained for the 0.94 and 0.52% alloys, respectively, for $E_{vs}{}^b = 0.08$ eV.

No. 11. Error in $E_{vs}{}^b$ due to inaccuracy in the solute concentration C_s. The mean concentrations of the bars are known to within ±0.02 at.% silver. Differentiating Eq. (2) with respect to C_s,

$$\frac{\delta E_{vs}{}^b}{E_{vs}{}^b} = \frac{kT[\exp(E_{vs}{}^b/kT) - 1]}{E_{vs}{}^b\exp(E_{vs}{}^b/kT)}\frac{|\delta C_s|}{C_s}. \quad \text{(B17)}$$

Equation (B17) gives 1.3 and 2.4% errors in $E_{vs}{}^b$ for the 0.94 and 0.52% alloys, respectively, for $E_{vs}{}^b = 0.08$ eV.

No. 12. Error due to uncertainty in vacancy concentration in pure aluminum, $C_v{}^0$. Differentiating Eq. (2) with respect to $C_v{}^0$,

$$\frac{\delta E_{vs}{}^b}{E_{vs}{}^b} = \frac{kT[\exp(E_{vs}{}^b/kT) - 1]}{E_{vs}{}^b\exp(E_{vs}{}^b/kT)}\frac{|\delta C_v{}^0|}{C_v{}^0}. \quad \text{(B18)}$$

The maximum value of $\delta C_v{}^0$ is $\pm4(10^{-5})$.[1] Errors of 3.2 and 3.0% in $E_{vs}{}^b$ are calculated for the 0.94 and 0.52% alloys, respectively, for $E_{vs}{}^b = 0.08$ eV.

No. 13. Error due to uncertainty in the absolute temperature T. Differentiating Eq. (2) with respect to T and evaluating the temperature dependence of ΔC_v and $C_v{}^0$ reveals an error in $E_{vs}{}^b$ of less than 0.5% in both alloys for an uncertainty in the absolute temperature of 2°C.

No. 14. Most probable total error. The most probable total error may be obtained by taking the square root of the sum of the squares of the above errors. For $E_{vs}{}^b = 0.08$ eV the most probable errors in ΔC_v calculated using error Nos. 1–9 are 29% in $\Delta C_v(643)$ for the 0.94% silver alloy and 51% in $\Delta C_v(650)$ for the 0.52% silver alloy. For $E_{vs}{}^b = 0.08$ eV the most probable errors in $E_{vs}{}^b$, calculated using error Nos. 10–13, are 18 and 32% for the 0.94 and 0.52% silver alloys, respectively.